JACS
JOURNAL OF THE AMERICAN CHEMICAL SOCIETY

COMMUNICATION

pubs.acs.org/JACS

# Microfluidic Generation of Multifunctional Quantum Dot Barcode Particles

Yuanjin Zhao,[†,‡] Ho Cheung Shum,[*,‡,§] Haosheng Chen,[‡,⊥] Laura L. A. Adams,[‡] Zhongze Gu,[*,†] and David A. Weitz[*,‡]

[†]State Key Laboratory of Bioelectronics, Southeast University, 210096 Nanjing, China

[‡]School of Engineering and Applied Sciences and Department of Physics, Harvard University, Cambridge, Massachusetts 02138, United States

[§]Department of Mechanical Engineering, The University of Hong Kong, 7/F Haking Wong Building, Pokfulam Road, Hong Kong

[⊥]State Key Laboratory of Tribology, Tsinghua University, Beijing 100084, China

Supporting Information  Web-Enhanced

**ABSTRACT:** We develop a new strategy to prepare quantum dot (QD) barcode particles by polymerizing double-emulsion droplets prepared in capillary microfluidic devices. The resultant barcode particles are composed of stable QD-tagged core particles surrounded by hydrogel shells. These particles exhibit uniform spectral characteristics and excellent coding capability, as confirmed by photoluminescence analyses. By using double-emulsion droplets with two inner droplets of distinct phases as templates, we have also fabricated anisotropic magnetic barcode particles with two separate cores or with a Janus core. These particles enable optical encoding and magnetic separation, thus making them excellent functional barcode particles in biomedical applications.

The increasing use of high-throughput assays in biomedical applications, including drug discovery and clinical diagnostics,[1,2] demands effective strategies for multiplexing. One promising strategy is to use barcode particles, which encode information about their specific compositions and enable simple identification. Many encoding strategies have been proposed for these barcode particles, including incorporation of segmented nanorods[3] and photopatterning[4−6] as well as the use of photonic crystals,[7,8] fluorescent silica colloids,[9] and semiconductor quantum dots (QDs).[10−16] In particular, semiconductor QDs hold immense promise as barcode elements because of their excellent optical properties, such as minimal spectral width and remarkable photostability. In addition, by mixing QDs with different emission wavelengths at different concentrations, significantly larger combinations can be interrogated with a single excitation wavelength. To generate barcodes, QDs can be incorporated into the particles before their polymerization or during their swelling,[10,14] The QDs can also be applied as a coating on the surface of the particles.[11,12] However, QD barcodes generated by this approach often suffer from leakage of QDs; this significantly affects the performance and stability of the barcode particles. In addition, traditional processes used for generating such particles provide little control over the characteristics of the result particles, such as particle sizes and number and distribution of QDs within each particles; thus, the resultant QD barcodes often have high variability of fluorescence intensities.[13−16] This is exacerbated by the uncontrolled motion of these barcode particles, which reduces the sensitivity of the assay[6] and demands more complicated procedures for enriching the barcode particles during assay.[17] These, together with the debatable biocompatibility of such particles, have limited their applications.[16] Thus, novel approaches for generating functional QD barcode particles are still needed.

Due to the ability to control the structures of the final emulsion, microfluidic techniques have emerged as a promising and versatile technique for generating monodisperse emulsion droplets. These have been applied to fabricate microgels, polymeric particles, compounds, and composite particles by using microfluidic emulsion droplets as templates.[18−23] These droplets have been prepared in typical lithography-based and capillary microfluidic devices. While lithography-based devices offer great potential for scaling up the production, capillary microfluidic techniques have demonstrated robustness in forming multiple emulsions for generating novel materials with the functions of encapsulation, confinement of microreactions, and sensing.[24−30] However, these approaches have not been applied to prepare barcode particles. By using multiple emulsions as particle templates, barcode elements, such as QDs, can be immobilized in structures templated by the emulsions and applied to solvents in which the elements are normally unstable. Due to the immobilization and enclosure by the shell layers of the emulsions, leakage of the barcode elements can be prevented. Moreover, by encapsulating additional functional elements in the emulsion templates, barcode particles with distinct functions, such as controllable movement and improved sensitivity, can be achieved.

In this paper, we describe a simple approach for generating barcode particles using capillary microfluidics. The prepared barcode particles are composed of QD-tagged resin cores and hydrogel shells. These barcodes have highly stable and uniform spectral characteristics and are biocompatible. By using double emulsions with multiple inner droplet phases, we have also fabricated anisotropic magnetic barcode particles with excellent control over their rotation and aggregation under different magnetic fields; this will significantly simplify the processing of

**Received:** January 25, 2011

   dx.doi.org/10.1021/ja200729w | J. Am. Chem. Soc. XXXX, XXX, 000–000

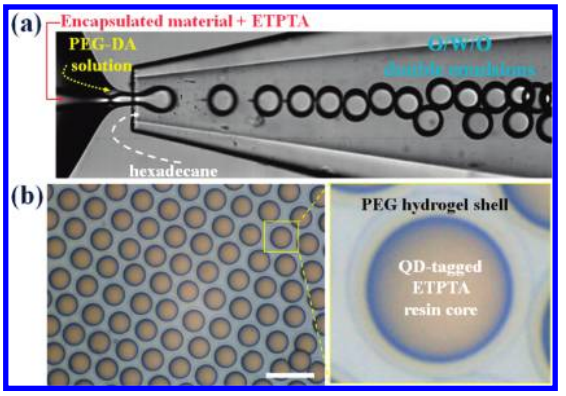


**Figure 1.** (a) Formation of O/W/O double emulsions in a glass microcapillary device. (b) Optical micrograph of the polymerized double emulsions with PEG hydrogel shells and QD-tagged ETPTA resin cores. Scale bar is 100 $\mu$m.

particle-based assays. These features make the barcode particles described here ideal for biomedical applications.

In a typical experiment, a capillary microfluidic double-emulsion device is assembled by aligning two cylindrical capillaries coaxially inside a square capillary.[24] By combining the co-flow and flow-focusing geometries, the device can be used for generating monodisperse oil-in-water-in-oil (O/W/O) double emulsions, as shown in Figure 1a. The inner oil phase is pumped through one tapered round capillary, while the middle aqueous phase flows through the region between the inner round capillary and the outer square capillary in the same direction. The inner oil droplets form by dripping from the tip of the inner round capillary in the co-flow geometry. The outer oil phase flows, in the opposite direction, through the region between the other round capillary, often known as the collection capillary, and the outer square capillary and hydrodynamically focuses the middle phase containing the innermost droplets; the resultant jet breaks up into monodisperse O/W/O double-emulsion drops at the orifice of the collection capillary.

In this work, the inner-most oil phase consists of QDs and silica colloidal nanoparticles dispersed in ethoxylated trimethylolpropane triacrylate (ETPTA); the silica colloidal nanoparticles are added to the inner ETPTA phase to prevent aggregation of the QDs and maintain a uniform distribution of the QDs in the ETPTA cores. The middle aqueous phase is made up of a poly(ethylene glycol) diacrylate (PEG-DA) solution with 0.25% w/w sodium dodecyl sulfate (SDS) and 0.25% w/w ethyleneoxide propyleneoxide triblock copolymer (Pluronic F108) for stabilizing the double emulsions. The outer oil phase is hexadecane with 2.5 wt % of ABIL EM 90 surfactant. Under these optimal conditions, double emulsions can be fabricated and, by adjusting the flow rates, can be made with sizes ranging from tens to hundreds of micrometers. With these O/W/O double emulsions as templates, the hydrophobic QDs are completely encapsulated in the innermost resin droplets surrounded by the middle aqueous shells; thus, leakage of the QDs can be prevented. By photopolymerizing the double-emulsion templates with UV illumination, monodisperse barcode particles with QD-tagged ETPTA resin cores and PEG hydrogel shells are generated, as shown in Figure 1b. The polymerized QD-containing particles are highly stable and can be washed, dried, and redispersed into water without damage. The PEG hydrogel shells of the particles are also stable and do not show any observable volume change

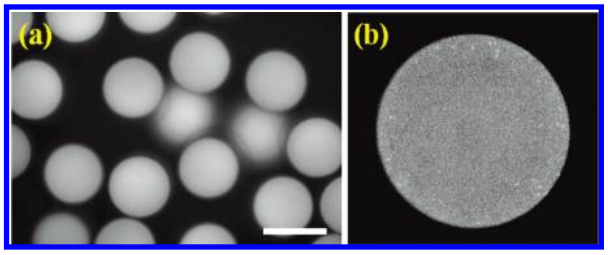


**Figure 2.** (a) Fluorescence image of the QD-containing barcode particles. (b) Laser scanning confocal microscope (LSCM) image of the QD-tagged particle core section. Scale bar is 50 $\mu$m.

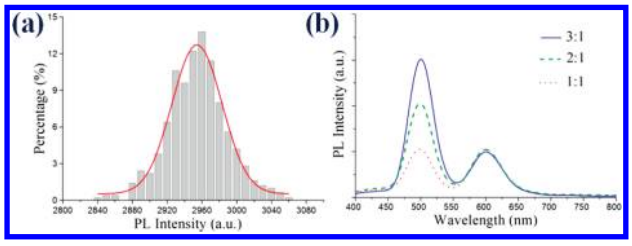


**Figure 3.** (a) Distribution of the PL intensities in the QD-containing (1 mg/mL) barcode particles. Polydispersity in the distribution of the intensities is less than 3.5%. The experimental data are fitted with a Gaussian distribution in red. (b) Representative spectra of barcode particles containing two types of QDs with different emission wavelengths mixed in ratios of 3:1, 2:1, and 1:1.

under neutral or near-neutral pH. Although the shells are permeable to aqueous solutions or some biomolecules, the QDs are locked firmly inside the cores due to the formation of the rigid ETPTA structure after polymerization.

These particles have many attributes that will make them excellent as barcode particles. This application requires the particles to have many optically distinguishable properties. Here, the QDs are uniformly dispersed in the core of the particles, as confirmed by the uniform fluorescence intensity over the particles shown in Figure 2. Based on the photoluminescence (PL) spectra of the QDs encapsulated, the barcode particles prepared can be easily distinguished by their PL intensities and wavelengths under a single excitation light. In our experiment, the inner ETPTA phases contain different types and concentrations of QDs. The PL intensity of our barcode particles increases with the concentration of QDs in the ETPTA resin, as demonstrated by the plot in Figure S1. Since the concentration of QDs that can be encapsulated into the particle cores is very high (5 mg/mL in this case), a wide range of barcode PL intensities can be achieved. Due to the low polydispersity of the barcode cores (about 2%), the uniform distribution of QDs, and the relatively large number of QDs in each particle, the PL intensities of the barcode particles have very low standard deviations of less than 3.5%, as shown in Figure 3a. These results indicate that more than 30 intensity levels can be achieved with a given color of QDs for the barcodes generation; this is higher than previously reported values using QDs for multiplexing.[10,16] The PL intensity levels of our barcode particles could be further increased by using much higher concentrations of QDs in the ETPTA resin for the particles fabrication. Additional coding can be achieved by using multiple types of QDs with different wavelengths.

To demonstrate the ability to distinguish PL from QDs with different wavelengths, we encapsulated two different types of


dx.doi.org/10.1021/ja200729w |J. Am. Chem. Soc. XXXX, XXX, 000–000

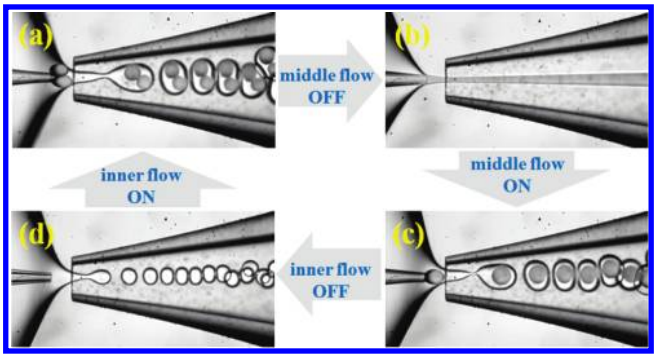


**Figure 4.** Formation of double emulsions with two distinct inner phases in a glass microcapillary device. The two inner phases is injected into the device separately through separate channels within the same round capillary. The two inner phases consist of QD- and magnetic nanoparticle-dispersed ETPTA fluids. (a) Formation of double-emulsion drops with two separate inner droplets; (b) formation of a Janus inner jet surrounded by the middle shell phase; (c) formation of double-emulsion drops with Janus inner droplets; and (d) formation of droplets of the middle phase.

QDs at varying ratios in the same particles. The peaks at different wavelengths in the PL spectrum can be distinguished clearly, as shown in Figure 3b. In our experiments, the barcodes are read out by using a microscope equipped with a fiber-optic spectrometer at a single UV excitation wavelength; for larger numbers of decoding levels, the process can be sped up using an automatic decoding machine. Theoretically, with $N$ intensity levels with $M$ colors, $(N^M - 1)$ unique codes can be generated. Therefore, a total of 899 different codes can be generated by using two types of QDs with 30 intensity levels (that is, $N = 30$ and $M = 2$) for each type of QDs. In practice, it is realistic to use three or four types of QDs with 30 intensity levels each, yielding 27 000−810 000 recognizable codes with a single excitation laser. These indicate the excellent capability of this encoding strategy in our barcode particles. Moreover, in our barcode particles, biomolecules can be immobilized in the shell layer for assays and reactions. Since the QDs are locked inside the solid resin and the QD-containing cores are surrounded by biocompatible PEG hydrogel shells, the biomolecules would not come into direct contact with the QDs, which can be toxic to them. Therefore, assays using our barcode particles for multiplexing could be applied to a much wider range of biomolecules.

To impart additional functionality to the barcode particles, we have also generated particles with more complex internal structures by using a capillary microfluidic device that enables separate injection of multiple inner phases,[31,32] as shown in Figure 4. For instance, magnetically anisotropic barcode particles can be fabricated by flowing QD-tagged ETPTA in one inner channel and ferric-oxide-containing ETPTA in the other inner channel. By tuning the flow rates and the composition of the phases, double-emulsion templates with two separate inner droplets (Figure 4a) and a single Janus droplet (Figure 4c) of QD- and ferric-oxide-containing ETPTA can be generated in the same microfluidic device. By using appropriate surfactants (SDS and Pluronic F108 in this case) in the middle aqueous phase, the inner droplets formed can remain highly stable without coalescence with each other (Figure 4a). Thus, the generation process of the double-emulsion templates with separate inner droplets can remain stable for a long time (Movie S1). Nevertheless, we can switch from having two separate inner droplets to having a single Janus inner droplet by turning the middle phase off temporarily. When the flow of the middle phase is stopped, the two inner ETPTA phases coalesce to form a single jet that has a Janus structure in the continuous phase (Figure 4b). When the flow of the middle phase is switched on again, the Janus jet is sheared into Janus inner droplets, which contain QD-tagged and ferric-oxide tagged ETPTA on the two faces (Figure 4c). Surprisingly, this generation mode can also remain stable (Movie S2). By turning the inner ETPTA phase off momentarily, we can also switch from having Janus cores back to having two separate cores. By stopping the flow of the innermost phases briefly, we form single droplets of the middle phase in the continuous phase (Figure 4d). When the flows of the inner phases are switched on again, two distinct types of inner droplets are formed again. In the presence of surfactants in the middle phase, coalescence between the two types of inner droplets is avoided, thus forming double-emulsion drops with two separate inner droplets, as shown in Figure 4a. The ability to change the structures of the emulsions simply by switching the flow on and off sequentially in the microfluidic device allows flexible on-demand generation of double-emulsion templates with desired structures.

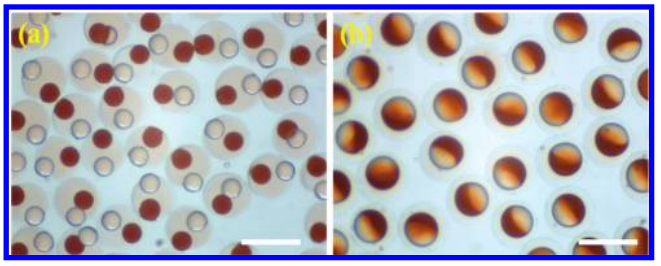


**Figure 5.** Bright-field microscope images of the polymerized double emulsions with (a) separate QD- and magnetic-nanoparticle-tagged ETPTA resin cores and (b) single Janus cores with a side consisting of QD-tagged ETPTA and another side of magnetic-nanoparticle-tagged ETPTA. The light part is the QD-tagged core, and the brown part is the magnetic-nanoparticle-tagged core. Scale bar is 200 $\mu$m.

With UV polymerization of the double-emulsion templates, we have generated barcode particles with two separate cores or a single Janus core consisting of a face of QD-tagged ETPTA and another face of magnetic-tagged ETPTA, as shown in Figure 5. By simply adjusting the flow rates of the two inner phases separately, we also form barcode particles with higher numbers of inner droplets, as shown in Figure S2. The QD-tagged ETPTA cores can be used for multiplexing, while the magnetic ETPTA cores allow controlled actuation of the particles by tuning the surrounding magnetic field. Since the QDs and ferric oxide nanoparticles in the barcode particles are separated, the fluorescence intensity of the QDs will not be attenuated by optical absorption of photons due to the ferric oxide nanoparticles;[15] thus, the stability of the coding PL intensities of the particles can be maintained. In addition, due to the anisotropic distribution of ferric oxide in the barcode particles, the particles rotate under a rotating magnetic field (Movie S3) and can be pulled to the side of a vial using a permanent magnet (as shown in Figure S3). This not only increases the sensitivity of the barcode particles (as shown in Figure S4) but also enables simple capture and enrichment of the barcode particles in bioassays, although the sensitivity toward binding of biomolecules may also depend on the size of the barcode particles. Therefore, our barcode particles have great potential for use in high-throughput bioassays that require barcode particles with high sensitivity and controllable motion.[6,17]


dx.doi.org/10.1021/ja200729w |J. Am. Chem. Soc. XXXX, XXX, 000–000

In conclusion, we have developed a new approach to prepare barcode particles by encapsulating QDs in double-emulsion templates generated in capillary microfluidic devices. The resultant particles exhibit uniform spectral characteristics and allow substantial numbers of coding levels for multiplexing. Moreover, the approach also enables fabrication of anisotropic magnetic barcode particles, which rotate under a rotating magnetic field and aggregate under a stationary magnetic field. These create new opportunities to perform magnetic separation of the barcode particles. The unique features of our QD-containing barcode particles make them highly promising as microcarriers in biomedical applications, including high-throughput bioassays and cell culture research where multiplexing is needed.

## ■ ASSOCIATED CONTENT

**Ⓢ Supporting Information.** Experimental procedures, photoluminescence spectra of the QD-containing barcode particles, microscope images of barcode particles with higher numbers of cores, and permanent magnet-induced particle separation. This material is available free of charge via the Internet at http://pubs.acs.org.

**Ⓦ Web Enhanced Feature.** Movies (.avi) of double microfluidic emulsions generation and barcode particles rotations are available in the HTML version. Movie S1 shows formation of double emulsions with two separate inner droplets. Movie S2 shows formation of double emulsions with single Janus inner droplets. Movie S3 shows rotation of the anisotropic magnetic barcode particles with two separate cores or with a Janus core under a rotating magnetic field.

## ■ AUTHOR INFORMATION

**Corresponding Author**
gu@seu.edu.cn (Z.Z.G.); weitz@seas.harvard.edu (D.A.W.); ashum@hku.hk (H.C.S.)

## ■ ACKNOWLEDGMENT

This research was supported by the 333 Talent Project Foundation and Qing Lan Project of Jiangsu Province, Jiangsu Science and Technology Department (Grant No. BE 2009148 and BE 2008318), National Science Foundation of China (Grant No. 50925309), NSF (DMR-1006546), and Harvard MRSEC (DMR-0820484). Y.Z. thanks the Scientific Research Foundation of Graduate School of Southeast University.

## ■ REFERENCES

(1) Wilson, R.; Cossins, A. R.; Spiller, D. G. *Angew. Chem. Int. Ed.* **2006**, *45*, 6104–6117.
(2) LaFratta, C. N.; Walt, D. R. *Chem. Rev.* **2008**, *108*, 614–637.
(3) Nicewarner-Pena, S. R.; Freeman, R. G.; Reiss, B. D.; He, L.; Pena, D. J.; Walton, I. D.; Cromer, R.; Keating, C. D.; Natan, M. J. *Science* **2001**, *294*, 137–141.
(4) Braeckmans, K.; de Smedt, S.; Roelant, C.; Leblans, M.; Pauwels, R.; Demeester, J. *Nat. Mater.* **2003**, *2*, 169–173.
(5) Pregibon, D. C.; Toner, M.; Doyle, P. S. *Science* **2007**, *315*, 1393–1396.
(6) Lee, H.; Kim, J.; Kim, H.; Kim, J.; Kwon, S. *Nat. Mater.* **2010**, *9*, 745–749.
(7) Cunin, F.; Schmedake, T. A.; Link, J. R.; Li, Y. Y.; Koh, J.; Bhatia, S. N.; Sailor, M. J. *Nat. Mater.* **2002**, *1*, 39–41.
(8) Zhao, Y. J.; Zhao, X. W.; Hu, J.; Li, J.; Xu, W. Y.; Gu, Z. Z. *Angew. Chem. Int. Ed.* **2009**, *48*, 7350–7352.
(9) Battersby, B. J.; Bryant, D.; Meutermans, W.; Matthews, D.; Smythe, M. L.; Trau, M. *J. Am. Chem. Soc.* **2000**, *122*, 2138–2139.
(10) Han, M. Y.; Gao, X. H.; Su, J. Z.; Nie, S. M. *Nat. Biotechnol.* **2001**, *19*, 631–615.
(11) Wang, D. Y.; Rogach, A. L.; Caruso, F. *Nano Lett.* **2002**, *2*, 857–861.
(12) Rauf, S.; Glidle, A.; Cooper, J. M. *Adv. Mater.* **2009**, *21*, 4020–4024.
(13) Gao, X. H.; Nie, S. M. *Anal. Chem.* **2004**, *76*, 2406–2410.
(14) Kuang, M.; Wang, D. Y.; Bao, H. B.; Gao, M. Y.; Mohwald, H.; Jiang, M. *Adv. Mater.* **2005**, *17*, 267–270.
(15) Sathe, T. R.; Agrawal, A.; Nie, S. *Anal. Chem.* **2006**, *78*, 5627–5632.
(16) Zrazhevskiy, P.; Sena, M.; Gao, X. H. *Chem. Soc. Rev.* **2010**, *39*, 4326–4354.
(17) Kim, S. H.; Sim, J. Y.; Lim, J. M.; Yang, S. M. *Angew. Chem. Int. Ed.* **2010**, *49*, 3786–3790.
(18) Tumarkin, E.; Kumacheva, E. *Chem. Soc. Rev.* **2009**, *8*, 2161–2168.
(19) Dinsmore, A. D.; Hsu, M. F.; Nikolaides, M. G.; Marquez, M.; Bausch, A. R.; Weitz, D. A. *Science* **2002**, *298*, 1006–1009.
(20) Theberge, A. B.; Courtois, F.; Schaerli, Y.; Fischlechner, M.; Abell, C.; Hollfelder, F.; Huck, W. T. S. *Angew. Chem. Int. Ed.* **2010**, *49*, 5846–5868.
(21) Choi, S. W.; Zhang, Y.; Xia, Y. N. *Adv. Funct. Mater.* **2009**, *19*, 2943–2949.
(22) Schabas, G.; Wang, C. W.; Oskooei, A.; Yusuf, H.; Moffitt, M. G.; Sinton, D. *Langmuir* **2008**, *24*, 10596–10603.
(23) Wang, C. W.; Oskooei, A.; Sinton, D.; Moffitt, M. G. *Langmuir* **2010**, *26*, 716–723.
(24) Utada, A. S.; Lorenceau, E.; Link, D. R.; Kaplan, P. D.; Stone, H. A.; Weitz, D. A. *Science* **2005**, *308*, 537–541.
(25) Hanson, J.; Chang, C. B.; Graves, S. M.; Li, Z.; Mason, T. G.; Deming, T. J. *Nature* **2008**, *455*, 85–88.
(26) Chu, L. Y.; Utada, A. S.; Shah, R. K.; Kim, J. W.; Weitz, D. A. *Angew. Chem. Int. Ed.* **2007**, *46*, 8970–8974.
(27) Shum, H. C.; Kim, J. W.; Weitz, D. A. *J. Am. Chem. Soc.* **2008**, *130*, 9543–9549.
(28) Shum, H. C.; Bandyopadhyay, A.; Bose, S.; Weitz, D. A. *Chem. Mater.* **2009**, *21*, 5548–5555.
(29) Kanai, T.; Lee, D.; Shum, H. C.; Shah, R. K.; Weitz, D. A. *Adv. Mater.* **2010**, *22*, 4998–5002.
(30) Kim, S. H.; Shim, J. W.; Yang, S. M. *Angew. Chem. Int. Ed.* **2011**, *50*, 1171–1174.
(31) Sun, B. J.; Shum, H. C.; Holtze, C.; Weitz, D. A. *ACS Appl. Mater. Interfaces* **2010**, *2*, 3411–3416.
(32) Shum, H. C.; Zhao, Y. J.; Kim, S. H.; Weitz, D. A. *Angew. Chem. Int. Ed.* **2011**, *50*, 1648–1351.